Journal of Materials Chemistry B

PAPER

View Article Online
View Journal | View Issue

Cite this: J. Mater. Chem. B, 2015, 3, 3062

Photodynamic therapy of oligoethylene glycol dendronized reduction-sensitive porphyrins†

Lei Xu,[a] Lichao Liu,[a] Feng Liu,[a] Wen Li,*[b] Ruobin Chen,[b] Yun Gao[a] and Weian Zhang*[a]

Received 7th February 2015,
Accepted 25th February 2015

DOI: 10.1039/c5tb00276a

www.rsc.org/MaterialsB

OEGylation of porphyrins *via* a disulfide linkage to form a novel class of dendritic porphyrin photosensitizers (PSs) is presented. These amphiphilic PSs possess precise molecular structures which could self-assemble into spherical aggregates in aqueous solutions. Their thermoresponsiveness was investigated using UV-Vis spectroscopy, and their reduction responsive properties were inspected using dynamic light scattering and TEM measurements. Moreover, the uptake of porphyrin-containing dendritic micelles by cells and release of reduction-sensitive PSs were investigated using flow cytometry and confocal laser scanning microscopy. The results showed that the cellular uptake of dendritic micelles was more than that of free porphyrin and the uptake process was time-dependent. Additionally, the phototoxicity of these dendritic PS micelles was investigated by MTT assay. It was found that dendritic micelles exhibited efficient phototoxicity to cancer cells while the free porphyrin had nearly no toxicity under light irradiation. All results indicate that these dendritic PSs are promising for photodynamic therapy.

Introduction

Photodynamic therapy (PDT) is a controllable treatment that involves a photosensitizer, oxygen and light.[1,2] After irradiation with light of appropriate wavelength, the activated photosensitizer generates cytotoxic species which can attack cellular components and lead to the apoptosis or necrosis of target cells.[3–7] Compared with traditional therapies of tumors such as chemotherapy, radiation therapy and surgery, PDT shows excellent advantages because of its controllable destruction of diseased tissue, fast healing process without scarring, fewer side effects and non-invasion.[8] Thus, PDT has aroused great interest over the past decade for the treatment of neoplasm in skin, bladder, brain, ovaries and so on.[9,10] So far, some photosensitizers for PDT such as Photofrin, Foscan, Visudyne, Levulan and Metvix have been investigated and clinical approval obtained.[11]

To date, nanostructured carriers including inorganic nanoparticles, micelles and liposomes have been developed for drug delivery systems, since they exhibit many unique features like increasing the solubility of hydrophobic drugs in aqueous solutions,[12] prolonging the circulation time in blood, selectively accumulating into the tumor site by enhancing permeability and retention (EPR) effect and decreasing side effects.[13–19] Among these nanostructured carriers for drug delivery systems, dendrimers are promising materials since they show characteristics of a highly branched, monodispersed, well-defined topological structure, and have a large amount of functional peripheral groups.[13,20–22] Drugs can be loaded on dendrimers *via* non-covalent interaction or covalent bonding with the functional groups. Actually, dendrimer-based therapeutics have been widely used in anti-neoplastic agents, bio-imaging, neutron capture therapy, photothermal therapy and photodynamic therapy.[23] For example, Aida *et al.* had exploited an iron(II) porphyrin 1-methylimidazole complex covalently encapsulated within a large aryl ether dendrimer cage, which afforded a long-lived dioxygen adduct.[24] Jang *et al.* had developed a dendritic micelle system for PDT, which consisted of 32 negative charges on the periphery of a third generation poly(benzyl ether) dendritic zinc porphyrin, and a poly(ethylene glycol)–poly(L-lysine) block copolymer in aqueous media.[25] Recently, we developed a novel class of oligoethylene glycol (OEG)-based dendrimers which showed attractive thermosensitivity with tunable phase transition temperatures (LCSTs).[26,27] These thermo-responsive OEGylated dendrimers were found to be nontoxic and biocompatible, and exhibited a promising application as drug delivery nanocarriers.[28]

Controlled and enhanced release of drugs at the pathological site has been proven to be a great challenge for drug delivery.[29] Traditional drug release processes are dependent on the diffusion-controlled, flow-controlled and swelling-controlled processes which have exhibited many drawbacks such as different

[a] Shanghai Key Laboratory of Functional Materials Chemistry, School of Materials Science and Engineering, East China University of Science and Technology, 130 Meilong Road, Shanghai 200237, P. R. China. E-mail: wazhang@ecust.edu.cn
[b] Laboratory of Polymer Chemistry, Department of Polymer Materials, College of Materials Science and Engineering, Shanghai University, Nanchen Street 333, Materials Building Room 433, Shanghai 200444, China. E-mail: wli@shu.edu.cn

† Electronic supplementary information (ESI) available: Experimental details and characterization data. See DOI: 10.1039/c5tb00276a

release rates and limiting selection of drug carriers.[30] Much effort has been devoted to the development of stimuli-responsive drug delivery systems which could be responsive to external stimuli including temperature, pH, enzyme, ultrasound, light, oxidation and reduction.[31–37] Disulfide-containing reduction-responsive nanocarriers have been well studied and used in stimuli-responsive drug delivery systems, which can be sensitive to free thiols such as glutathione (GSH).[38–40] An important feature for fabrication of disulfide-containing drug delivery systems is the overexpression of GSH with abundant thiols in cancer cells compared with that in normal cells.[41] The concentration of GSH in the intracellular compartment (about 10 mM) is much higher than that in the extracellular compartment.[42] Therefore, disulfide-containing nanostructured carriers have received a considerable interest for intracellular release of the encapsulated drugs.[43–48]

Herein, a novel class of disulfide reduction-responsive dendritic amphiphilic drug carriers were constructed for PDT from ethoxyl-terminated first or second generation OEG dendrons, Et-G*n* (*n* = 1, 2), with 5-(4-hydroxylphenyl)-10,15,20-triphenylporphyrin (TPP-OH). The self-assembly behaviour of these porphyrin disulfides Et-G*n* (TPP-S-S-G*n*) in aqueous solutions was studied, and their thermo- and reduction-responsive behaviors were investigated by DLS and TEM. Flow cytometry and CLSM were further employed to monitor their location and uptake quantity by checking the fluorescence of porphyrin. The phototoxicity of these porphyrin dendritic micelles was evaluated by MTT assay against MCF-7 cells.

Experimental

Materials

Et-G1-OH, Et-G2-OH[49] and 5-(4-hydroxylphenyl)-10,15,20-triphenylporphyrin (TPP-OH)[50] were synthesized according to the previous studies, respectively. Dichloromethane (DCM) was dried over CaH_2 and distilled just before use. 1-(3-Dimethylaminopropyl)-3-ethylcarbodiimide hydrochloride (EDC), 4-dimethylaminopyridine (DMAP), 4′,6-diamidino-2-phenylindole (DAPI) and 3-(4,5-dimethylthiazol-2-yl)-2,5-diphenyltetrazolium bromide (MTT) were purchased from Aladdin and used as received. All other chemicals were of analytical grade and used as received unless mentioned.

Characterization

The proton NMR spectra were acquired using a Bruker 400 MHz NMR spectrometer using $CDCl_3$ as the solvent. UV-Vis spectra were recorded on a UV-2450 UV-Visible spectrophotometer with a temperature controlled water bath. Transmittance was monitored at a temperature increment of 1 °C with an equilibration time of 10 min, and 500 nm was monitored for transmission measurements with a solution concentration of 0.1 mg mL^{-1}. The fluorescence spectra were recorded on a F-4500 fluorescence spectrophotometer at room temperature. A BECKMAN COULTER Delsa Nano C particle analyzer was used to obtain the hydrodynamic diameter at a fixed angle of 165° at room temperature. TEM images were taken on a JEOL JEM1400 electron microscope operating at 100 kV. TEM samples were prepared by dropping the micelle solution (1 mg mL^{-1}) onto a carbon coated copper grid and which was then dried at room temperature.

Synthesis of 6-porphyrin-1-hexanol (TPPC6-OH). TPP-OH (0.63 g, 1 mmol), 6-chloro-1-hexanol (0.15 mL, 1.15 mmol) and potassium carbonate (0.14 g, 1 mmol) were mixed in DMF (100 mL). The mixture was refluxed for 12 h and washed with water three times. The product was extracted with DCM, and dried with anhydrous $MgSO_4$. After the solvent was removed by vacuum evaporation, the crude product was purified on a silica gel column with DCM as the eluent. Yield: 0.67 g (91.8%). ^{1}H NMR (400 MHz, $CDCl_3$), δ ppm: 8.87 (m, 8H, β-H), 8.21 (m, 6H, 10,15,20-Ar-*o*-H), 8.11 (m, 2H, 5-Ar-*o*-H), 7.76 (m, 9H, 10,15,20-Ar-*m*- and *p*-H), 7.28 (m, 2H, 5-Ar-*m*-H), 4.26 (t, 2H, –O–CH_2–CH_2–), 3.75 (t, 2H, –CH_2–OH), 2.00 (m, 2H, –O–CH_2–CH_2–CH_2–), 1.76–1.59 (m, 6H, –CH_2–CH_2–CH_2–CH_2–CH_2–OH), −2.77 (s, 2H, –N*H*–).

Synthesis of disulfide-modified carboxyl terminal porphyrin (TPP-S-S-COOH). TPP-S-S-COOH was synthesized *via* esterification by coupling TPPC6-OH with 3,3′-dithiodipropionic acid. Typically, TPPC6-OH (1.34 g, 2 mmol), 3,3′-dithiodipropionic acid (0.84 g, 4 mmol) and DMAP (0.246 g, 2 mmol) were dissolved in anhydrous DMF (50 mL) under a N_2 atmosphere. After the solution was cooled to 0 °C in an ice-water bath, DCC (0.82 g, 4 mmol) in DMF (5 mL) was added dropwise, and the mixture was stirred at room temperature overnight. Then the mixture was filtered to remove dicyclohexylurea, washed with DCM and brine, and dried with $MgSO_4$. After removing DCM by evaporation, the crude product was purified on a silica gel column with petroleum ether/ethyl acetate (3 : 2, v/v) as the eluent. Yield: 1.61 g (87.1%). ^{1}H NMR (400 MHz, $CDCl_3$), δ ppm: 8.87 (m, 8H, β-H), 8.21 (m, 6H, 10,15,20-Ar-*o*-H), 8.11 (m, 2H, 5-Ar-*o*-H), 7.76 (m, 9H, 10,15,20-Ar-*m*- and *p*-H), 7.27 (m, 2H, 5-Ar-*m*-H), 4.26 (t, 2H, –O–CH_2–CH_2–), 4.20 (t, 2H, –CH_2–CH_2–O–), 2.96 (m, 4H, –CH_2–CH_2–S– and –S–CH_2–CH_2–), 2.76 (–CO–CH_2–CH_2– and –CH_2–CH_2–CO–) 1.99 (m, 2H, –O–CH_2–CH_2–CH_2–), 1.84–1.74 (m, 6H, –CH_2–CH_2–CH_2–CH_2–CH_2–O–), −2.77 (s, 2H, –N*H*–).

Synthesis of porphyrin disulfide coupled Et-G*n* (*n* = 1, 2) (TPP-S-S-G*n*). A representative example for the synthesis of TPP-S-S-G*n* is as follows: TPP-S-S-COOH (0.923 g, 1 mmol), Et-G2-OH (2.409 g, 1 mmol), DMAP (0.0061 g, 0.5 mmol) and dry DCM (20 mL) were added into a dry bottle under N_2, and EDC (0.192 g, 1 mmol) in DCM (5 mL) was added drop-wise into the bottle in an ice-water bath. After the mixture was stirred at room temperature overnight, the mixture was washed with water, dried with $MgSO_4$ and filtered. After evaporation of the solvent, the crude product was purified on a silica gel column with petroleum ether/ethyl acetate (1 : 2 v/v) as the eluent. Yield: 2.26 g (67.9%). ^{1}H NMR (400 MHz, $CDCl_3$), δ ppm: 8.87 (m, 8H, β-H), 8.21 (m, 6H, 10,15,20-Ar-*o*-H), 8.11 (m, 2H, 5-Ar-*o*-H), 7.75 (m, 9H, 10,15,20-Ar-*m*- and *p*-H), 7.28 (m, 2H, 5-Ar-*m*-H), 6.64–6.48 (m, 8H, CH), 5.01 (s, 2H, –CO–O–CH_2–CH–), 4.43 (s, 6H, –O–CH_2–CH–), 4.26 (t, 2H, –O–CH_2–CH_2–CH_2–), 4.21 (m, 2H, –CH_2–CH_2–O–), 4.19–4.07 (m, 24H, –CH–O–CH_2–CH_2–), 3.89–3.45 (m, 138H, –O–CH_2–CH_2–O–CH_2–CH_2–O–CH_2–CH_2–O–CH_2–CH_3), 2.95 (t, 4H, –CH_2–CH_2–S– and –S–CH_2–CH_2–), 2.78 (q, 4H, –CO–CH_2–CH_2– and –CH_2–CH_2–CO–), 2.00 (m, 2H, –O–CH_2–CH_2–CH_2–), 1.84–1.64 (m, 6H, –O–CH_2–CH_2–CH_2–CH_2–CH_2–CH_2–O–), 1.20 (t, 27H, –CH_2–

CH_3), −2.77 (s, 2H, –N*H*–). MALDI-TOF-MS spectrum for TPP-S-S-G2, calcd for $C_{174}H_{254}N_4O_{53}S_2$, 3314.04; found 3312.51 (Fig. S5, ESI†).

Self-assembly of TPP-S-S-G*n* in aqueous solution. TPP-S-S-G*n* in THF (0.5 mL, 2 mg mL^{-1}) was added dropwise into water and then gradually dialyzed against water using a dialysis membrane (MWCO = 12 000) to remove THF. Dialysis was repeated at least three times to make sure that THF was removed completely.

Pyrene was used as a fluorescent probe to determine the critical micelle concentration (CMC). The concentration of TPP-S-S-G*n* was varied from 0.0002 mg mL^{-1} to 0.01 mg mL^{-1}, while the concentration of pyrene was fixed at 1 μM. The fluorescence spectra were recorded using a F-4500 fluorescence spectrometer with an excitation wavelength of 335 nm. The emission fluorescence at 372 and 383 nm was monitored for the calculation of the critical micelle concentration.

Fluorescence quantum yields

The fluorescence quantum yield (Φ_u) of TPP-S-S-G*n* micelles was measured by a comparative method using H_2TPP as a standard using eqn (1)[51,52]

$$\Phi_u = \Phi_s \frac{A_u I_u \lambda_s n_u^2}{A_u I_u \lambda_u n_s^2} \quad (1)$$

where Φ is the fluorescence quantum yield; I is the absorbance; A is the integrated fluorescence intensity; λ is the excitation wavelength and n is the refractive index of solution. The subscript "s" and "u" represent the standard and the sample, respectively.

Singlet oxygen quantum yields

The singlet oxygen quantum yield (Φ_Δ) was calculated according to the previous literature.[53–55] 1,3-Diphenylisobenzofuran (DPBF) was used as a scavenger to determine Φ_Δ. The quantum yield of $^1O_2$ generation by TPP-S-S-G*n* was determined by comparing with H_2TPP as a standard, which has a quantum yield of 0.62 in CCl_4. The DPBF decay at 410 nm was monitored every 10 s. The singlet oxygen quantum yield was calculated according to eqn (2):

$$\Phi_\Delta = \Phi_\Delta^{Std} \frac{R I_{abs}^{Std}}{R^{Std} I_{abs}} \quad (2)$$

where Φ_Δ^{Std} is the singlet oxygen quantum yield for the standard H_2TPP (Φ_Δ^{Std} = 0.62 in CCl_4); R and R^{Std} are the DPBF photobleaching rates in the presence of the analyte and the standard, respectively; I_{abs} and I_{abs}^{Std} are the rates of light absorption by the analyte and the standard, respectively. The concentration of the quencher (DPBF) was lower than 3×10^{-5} M to avoid chain reactions induced by quenchers (DPBF) in the presence of singlet oxygen. The experiments were carried out in CCl_4.

Reduction-destabilization of TPP-S-S-G*n* micelles. A TPP-S-S-G*n* micelle aqueous solution (1 mg mL^{-1}) was mixed with dithiothreitol (DTT) (10 mM) in PBS (pH = 7.4) solution, and then the mixed solvent was placed in a shaking bed at 37 °C with a rotation speed of 100 rpm. The size of the micelles was checked by DLS measurement at different times (4 h and 24 h).

Reduction-release of porphyrin from TPP-S-S-G*n* micelles. The release profiles of porphyrin from TPP-S-S-G*n* were studied using a membrane tubing (MWCO = 12 000) and immersed in a glass bottle containing PBS (pH = 7.4, 20 mL) or PBS with DTT (10 mM) in a shaking bed at 37 °C. At desired time intervals, 1 mL of an external buffer solution was taken out and replenished with an equal volume of fresh media. The amount of porphyrin released was determined using HPLC with a C18 Eclipse-XDB column (250 mm × 4.6 mm). The mobile phase was pure acetonitrile, and the flow rate was maintained at 1.0 mL min^{-1} and the detection wavelength was 420 nm. The release experiments were carried out in triplicate. Before this analysis, the standard curve of porphyrin was calibrated by HPLC. The control experiment was also carried out without DDT.

Cell culture

MCF-7 cells (human breast adenocarcinoma line) were cultivated in DMEM (Dulbecco's modified Eagle's medium) containing 10% FBS (fetal bovine serum) and 1% antibiotics (50 units per mL penicillin and 50 units per mL streptomycin) at 37 °C in a humidified atmosphere containing 5% CO_2. Cells were then treated with the medium containing various micelles or free porphyrin at different doses.

Intracellular uptake

MCF-7 cells were seeded on sterile cover glasses in a 6-well plate at a density of 1×10^5 cells per well and incubated overnight. Then the culture medium was replaced by fresh medium containing free porphyrin or TPP-S-S-G*n* micelles and incubated for 4 h and 24 h, respectively. Cells were fixed with 4% paraformaldehyde in PBS (pH = 7.4) for 30 min and washed 3 times with PBS, and then stained with 4′,6-diamidino-2-phenylindole (DAPI) to mark the nuclei. The cover glasses were placed onto slides for confocal laser scanning microscopy (CLSM) observation which was performed using a fluorescence microscope (Nikon AIR).

Fluorescence-activated cell sorting (FACS) was also employed to monitor the cellular uptake of free porphyrin and TPP-S-S-G*n* micelles, respectively. MCF-7 cells were seeded into a 6-well plate at the density of 1×10^6 cells per well and incubated for 4 h and 24 h, respectively. After predetermined time, the cells were washed, harvested and resuspended with PBS and then monitored by fluorescence-activated cell sorting using a FACScan flow cytometer (BD LSRFortessa). 10 000 cells were counted for each sample and the fluorescence of porphyrin was checked.

In vitro dark cytotoxicity and phototoxicity of TPP-S-S-G*n* micelles

The cell suspension (200 μL) of MCF-7 with a density of 7000 cells per well was seeded into a 96-well plate. After being incubated for 24 h, the MCF-7 cells were treated with different doses of free porphyrin and P-S-S-G*n* micelles in FBS-free DMEM at 37 °C for 24 h, and then the media were replaced with fresh DMEM culture medium. The cells were irradiated using a light emitting diode (LED) lamp (400 mW cm^{-2}) for 20 min and then incubated for 24 h. 20 μL of 3-(4,5-dimethylthiazol-2-yl)-2,5-diphenyltetrazolium bromide (MTT) solution (5 mg mL^{-1}) was added to each well for a further incubation of 4 h, followed by replacement with 150 μL DMSO to extract the formazan products by gentle agitation for 10 min. The absorbance at 560 nm was detected using a

spectrophotometric microplate reader (SpectraMax). The cell viability was calculated as follows: cell viability (%) = $(OD_{test} - OD_{background})/(OD_{control} - OD_{background}) \times 100$, where OD_{test} and $OD_{control}$ are, respectively, the absorbance in the presence of sample solutions and that without treatment. The *in vitro* dark cytotoxicity of TPP-S-S-G*n* or free porphyrin was checked using the same procedure as the phototoxicity of TPP-S-S-G*n* described above but without illumination.

To observe the PDT efficiency directly, MCF-7 cells were also stained with calcein-AM and PI after irradiation. MCF-7 cells were seeded onto a 6-well plate with 2×10^5 cells per well and incubated for 24 h. Then the medium was replaced by fresh medium containing 100 μg mL^{-1} porphyrin or fresh medium without micelles as a control. After incubation for another 24 h in the dark, the cells were irradiated with light for 20 min. After irradiation, the cells were further incubated for 24 h, and then washed with PBS and stained with calcein-AM and PI. All the cell experiments were repeated three times.

Results and discussion

Synthesis of porphyrin disulfide coupled G*n*-Et (*n* = 1, 2) (TPP-S-S-G*n*)

The synthesis routes for TPP-S-S-G2 are shown in Scheme 1. TPPC6-OH was firstly prepared from TPP-OH by etherification with 6-chloro-1-hexanol in DMF at 100 °C for 12 h. The ^{1}H NMR of TPPC6-OH is shown in Fig. S1 (ESI†). The proton signals at δ = 4.26, 3.75 and 2.0 are attributed to the methylene protons from –O–CH_2–CH_2–, –CH_2–OH and –O–CH_2–CH_2–CH_2– of the TPPC6-OH moiety, respectively. The hydroxyl group of TPPC6-OH was then changed to the carboxyl group by esterification with 3,3′-dithiodipropionic acid at room temperature. Here, the disulfide bond was introduced into this system, which is reduction-sensitive to GSH. After the esterification reaction, the methylene proton signal at 3.75 ppm (peak h in Fig. S1, ESI†) shifts to 4.20 ppm (peak g in Fig. S2, ESI†), and two new signals appear at 2.96 and 2.76 ppm, which are ascribed to methylene protons adjacent to disulphide and carbonyl groups.

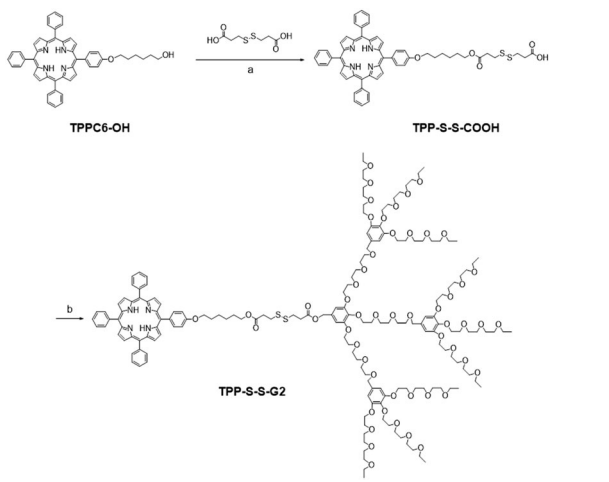

Scheme 1 Synthesis of the TPP-S-S-G2. (a) DCC/DMAP, R.T., 24 h; (b) Et-G2-OH, EDC/DMAP, R.T., 24 h.

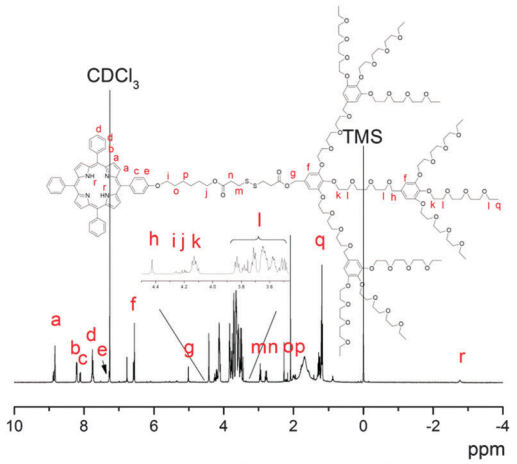

Fig. 1 ^{1}H-NMR spectrum of TPP-S-S-G2 in $CDCl_3$.

The three-folded oligoethylene glycol-based dendrons Et-G1-OH and Et-G2-OH exhibited attractive properties such as amphiphilicity, biocompatibility and thermoresponsiveness. TPP-S-S-COOH was attached to these dendrons through the esterification reaction in the presence of EDC/DMAP. The ^{1}H NMR spectrum of TPP-S-S-G2 is shown in Fig. 1. The proton signals at δ = 3.89–3.45 and 1.2 ppm are ascribed to the methylene groups and the terminal methyl groups of OEG, respectively, and the proton signals at δ = 5.01 and 4.43 ppm belong to benzyl of the OEG dendron moiety. The proton signals at δ = 8.87, 8.21, 8.11, 7.75, 7.28 and −2.77 ppm are all attributed to the porphyrin ring. Moreover, the integral area ratio of the imino group (peak a) with the methyl group (peak q) is almost equal to the theoretical value (1 : 9). Thus, ^{1}H NMR results clearly confirmed the successful synthesis of TPP-S-S-G2. TPP-S-S-G1 was also successfully prepared and its structure confirmed by the ^{1}H NMR spectrum (Fig. S3, ESI†).

Formation and reduction-responsive disruption of TPP-S-S-G*n* micelles in water

Micelles were prepared by adding the TPP-S-S-G*n*–THF solution dropwise into water and then dialyzed against water to remove THF. The critical micelle concentration (CMC) was determined using pyrene as a fluorescent probe. In an aqueous solution, pyrene can be transferred into the hydrophobic interior of micelles and results in significant spectroscopic changes. The ratio of pyrene fluorescence intensities excited at 383 and 372 nm (I_{383}/I_{372}) was plotted as a function of the logarithm of the concentration of TPP-S-S-G*n* micelles. As shown in Fig. 2, the ratio of I_{383}/I_{372} increases slowly at low concentration but increases sharply after the concentration reached a certain value, which indicates the formation of micelles. Finally, the CMC value of TPP-S-S-G1 and P-S-S-G2 was 1.71×10^{-3} mg mL^{-1} and 2.57×10^{-3} mg mL^{-1}, respectively. P-S-S-G2 has a higher CMC, since it has a larger hydrophilic segment of OEG.

TEM and DLS were employed to study reduction properties of TPP-S-S-G*n* micelles in response to 10 mM DTT. TEM images (Fig. 4a and d) show that TPP-S-S-G1 and TPP-S-S-G2 could form

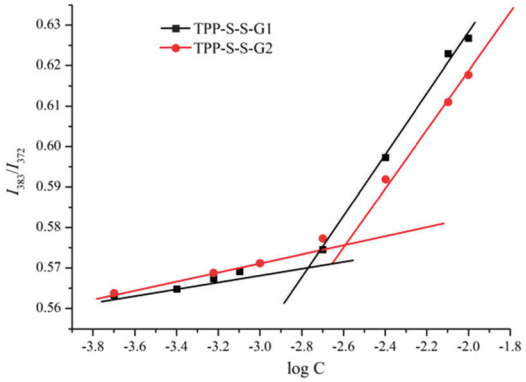

Fig. 2 Fluorescence intensity ratio I_{383}/I_{372} of pyrene as a function of logarithm of TPP-S-S-G*n* concentration.

spherical aggregates in water. Moreover, the size of TPP-S-S-G2 micelles is slightly bigger than that of TPP-S-S-G1 micelles, which could have resulted from the structures of the G2 dendrons. TPP-S-S-G2 has long OEG chains, leading to a bigger corona. In this system, the reduction-responsive disulfide bond was introduced into dendritic molecules, which could be broken by GSH in cancer cells. It is well-known that DTT could oxidize the disulfide bond of the dendrimer and disrupt the micelles. After treating with DTT, the spherical micelles were destroyed and some aggregates were formed at 4 h and 24 h. As shown in Fig. 4b, c, e and f, the spherical aggregates of TPP-S-S-G*n* were disrupted by DTT to form larger aggregates. DLS was also used to characterize these micelles, and the results showed that the diameter of TPP-S-S-G1 micelles was 116.4 nm with PDI = 0.166 and that of TPP-S-S-G2 was 126.6 with PDI = 0.227. After TPP-S-S-G*n* micelles were treated with DTT for 4 h, the main scattering peak shifts to a higher diameter, accompanied by the appearance of a new small peak in the lower diameter range (Fig. 3). Moreover, when treated with DTT for 24 h, there is not only a small peak in the range of lower diameter, but also the main scattering peak becomes much broader, and a big shoulder appears in the peak, suggesting that the micelles were disrupted by DTT. A similar result was also observed for TPP-S-S-G1 micelles (Fig. S6, ESI†). For comparison, the stability of TPP-S-S-G*n* micelles after 24 h in the absence of DTT under the same conditions was also studied by DLS, and the results showed that the diameter and PDI of TPP-S-S-G*n* micelles showed nearly no change.

The stability and zeta potential of TPP-S-S-G*n* micelles in PBS and DMEM at 37 °C were further evaluated, respectively. As shown in Fig. S7 and Table S1 (ESI†), the two kinds of micelles were all quite stable in PBS for 10 days besides the PDI of TPP-S-S-G2 micelles became broad. For the TPP-S-S-G*n* micelles in DMEM, it can be seen that the smaller peaks appeared in the lower diameter range, but the main peaks were very similar to that of micelles in water or PBS. The appearance of small peaks should have resulted due to the formation of the small particles. After 10 days, TPP-S-S-G1 micelles in DMEM were also quite stable except for some change of the small aggregates. However, for TPP-S-S-G2 micelles in DMEM, the PDI obviously became broad, although the size of the aggregates did not increase after 10 days. Additionally, the zeta potential of TPP-S-S-G1 and TPP-S-S-G2 micelles in PBS was −34.42 mV and −29.34 mV, and then changed to −13.26 mV and −16.81 mV after 10 days, respectively. The decrease in the zeta potential of TPP-S-S-G*n* micelles was also found in DMEM, which further confirms the DLS results.

Thermoresponsive behavior

The thermoresponsiveness of these two dendritic TPP-S-S-G*n* was, respectively, evaluated in aqueous solutions by checking the transmittance at 550 nm. As shown in Fig. 5, both TPP-S-S-G1 and TPP-S-S-G2 are thermoresponsive and show abrupt phase transitions with their LCSTs at 32.4 °C and 35.8 °C, respectively. Their LCSTs were dependent on the mass ratio of the hydrophilic OEG dendrons to hydrophobic porphyrin. TPP-S-S-G2 contains more OEG units than TPP-S-S-G1, which means that TPP-S-S-G2 is more hydrophilic, resulting in a higher LCST.

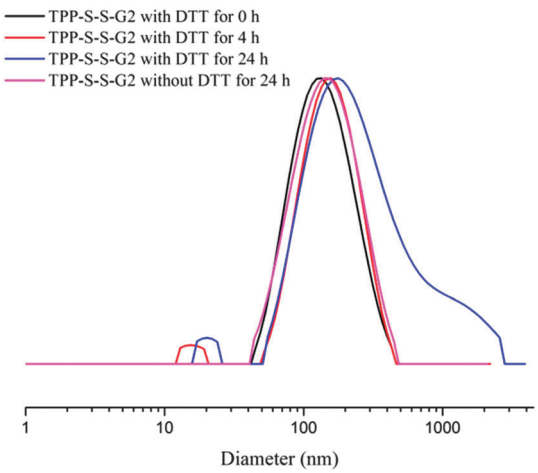

Fig. 3 Size distribution of TPP-S-S-G2 micelles determined by DLS. Blank line: DTT for 0 h, red line: DTT for 4 h, green line: DTT for 24 h, pink line: without DTT for 24 h.

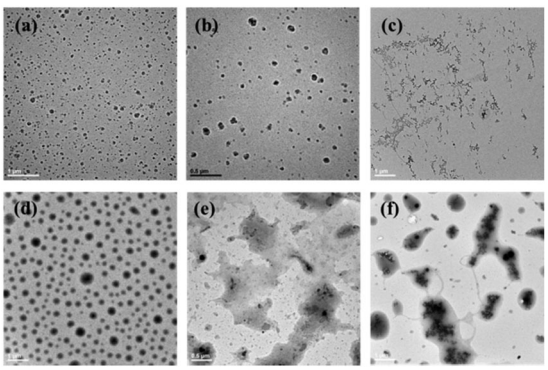

Fig. 4 TEM images of TPP-S-S-G1 (a–c) and TPP-S-S-G2 micelles (d–f) with treatment using DDT at different times; (a and d) DTT for 0 h (scale bar, 1 μm), (b and e) DTT for 4 h (scale bar, 0.5 μm), and (c and f) DTT for 24 h (scale bar, 1 μm).

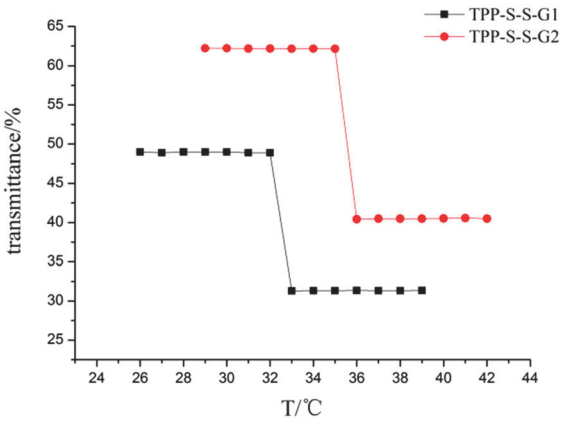

Fig. 5 Temperature dependences of transmittance at 550 nm obtained for aqueous solutions of TPP-S-S-G1 (0.1 mg mL^{-1}) and TPP-S-S-G2 (0.1 mg mL^{-1}).

Below LCST, OEG chains were surrounded with water molecules to ensure their water solubility. When the temperature was above LCST, the bound water molecules escaped from OEG chains and these chains tended to shrink.[56] The entropy gain in the process of bound water released from TPP-S-S-G2 was higher than that of TPP-S-S-G1 which was compensated by temperature.[57] So the LCST of TPP-S-S-G*n* was mainly dependent on the mass ratio of the hydrophilic OEG dendrons to hydrophobic porphyrin.

Fluorescence quantum yields and singlet oxygen quantum yields

The fluorescence quantum yield of these two TPP-S-S-G*n* dendritic micelles in water was checked using a UV and a fluorescence spectrophotometer by using H_2TPP as the standard, and the results are shown in Fig. 6. According to eqn (1), the fluorescence quantum yields of TPP-S-S-G1 and TPP-S-S-G2 were 0.011 and 0.028, respectively, which were 5–10 fold lower than that of the control H_2TPP (0.11). Additionally, the UV-Vis spectra (Fig. 6a) of TPP-S-S-G1 and TPP-S-S-G2 micelles showed that the micelles exhibited a clear red shift compared to the H_2TPP–THF solution. The red shift indicates that the porphyrin moieties were π-stacking with each other in the micelle core, which causes the decrease of the fluorescence quantum yield.

The singlet oxygen quantum yields of TPP-S-S-G*n* were also measured. After irradiation, the energy transferred from the excited triplet state of porphyrin to the ground state of oxygen to generate singlet oxygen. DPBF was used to capture singlet oxygen, and the peak intensity of the mixture of DPBF and TPP-S-S-G*n* in CCl_4 was checked using a UV-Vis spectrophotometer (Fig. 7). The singlet oxygen quantum yield of TPP-S-S-G1 and TPP-S-S-G2 was 0.614 and 0.623, respectively, which was calculated according to eqn (2). Thus, these two dendritic porphyrin derivatives showed a similar singlet oxygen quantum yield compared to H_2TPP (0.62).

Reduction-release of porphyrin from TPP-S-S-G*n* micelles

In vitro release of porphyrin from TPP-S-S-G*n* micelles was investigated using a dialysis tube (MWCO = 12 000) in PBS

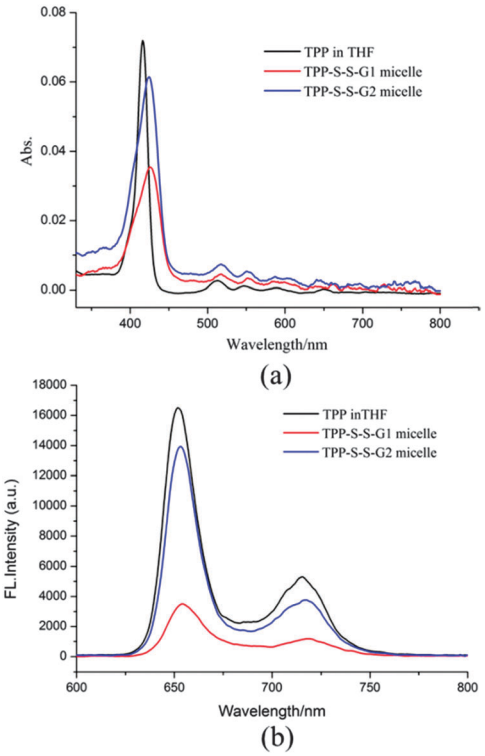

Fig. 6 (a) UV-Vis absorption spectra of TPP-S-S-G*n* micelles in pure water, and (b) fluorescence emission spectra of TPP-S-S-G*n* micelles.

buffer (pH = 7.4) at 37 °C by gentle shaking in the presence or absence of 10 mM DTT. As shown in Fig. 8, TPP-S-S-G1 and TPP-S-S-G2 micelles have a similar release behavior to porphyrin under the same conditions. At the first 20 h, the porphyrin showed a rapid release rate, and about 60% porphyrins were released upon treatment with 10 mM DTT. In contrast, there is nearly no porphyrin released from the TPP-S-S-G*n* micelles without treatment with DTT. Thus, the result of *in vitro* drug release clearly demonstrated that these micelles were reduction-responsive, which could effectively release porphyrin moieties in response to GSH inside the cells.

In vitro cellular uptake of TPP-S-S-G*n* micelles

The cellular uptake and intracellular distribution of free porphyrin and TPP-S-S-G*n* micelles *in vitro* were evaluated using MCF-7 by flow cytometry and confocal laser scanning microscopy, respectively (Scheme 2). For quantitative determination of the fluorescence of porphyrin inside cells, the TPP-S-S-G*n* micelles were added to the culture medium with a porphyrin concentration of 50 μg mL^{-1} and cells were incubated for 4 h and 24 h. As shown in Fig. 9, after 4 h incubation with free porphyrin and TPP-S-S-G2 micelles, we could clearly see that the fluorescence intensity of TPP-S-S-G2 micelles was higher than that of the control, indicating that the cells had taken in porphyrin and TPP-S-S-G2 micelles. Moreover, the fluorescence peak of TPP-S-S-G2 micelles shifts to the right compared to that of free porphyrin at the same incubation time, which means that more TPP-S-S-G2 micelles had been up-taken than free

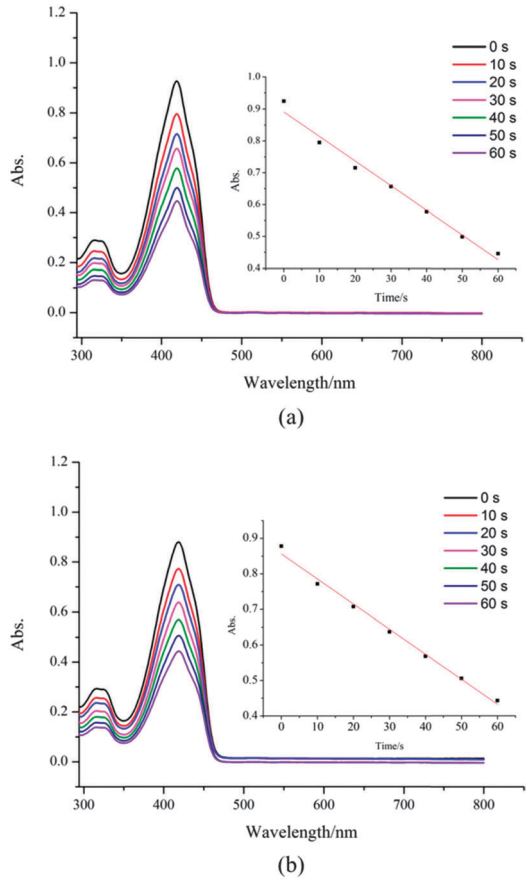

Fig. 7 UV-Vis absorption spectra of DPBF with (a) TPP-S-S-G1 and (b) TPP-S-S-G2 after irradiation at different times in CCl_4 (inset: plot of absorbance *versus* time).

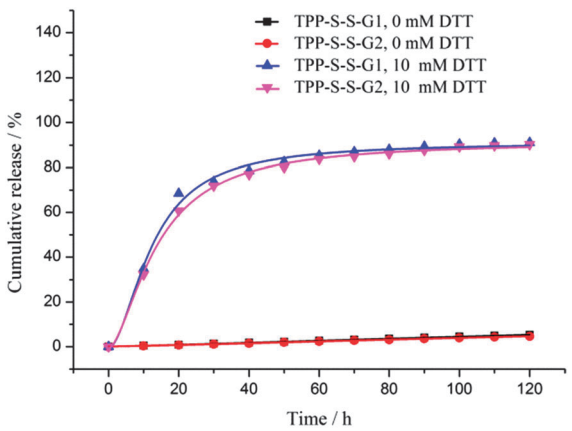

Fig. 8 The reduction behavior of porphyrin released from TPP-S-S-G1 and TPP-S-S-G2 micelles with and without the treatment of DTT. The profiles of porphyrin were recorded at 37 °C with pH = 7.4.

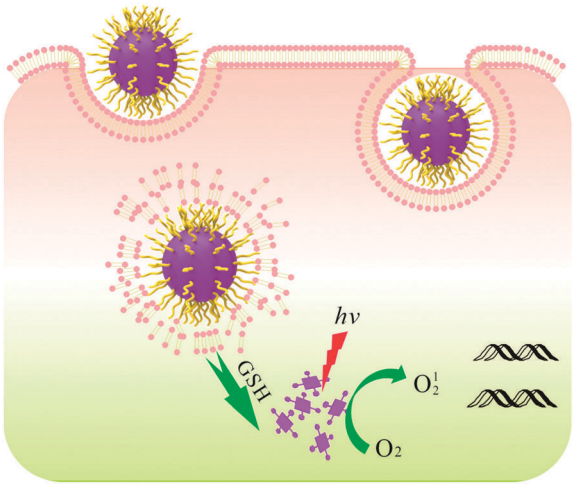

Scheme 2 Illustration of TPP-S-S-G*n* micelles for intracellular PDT.

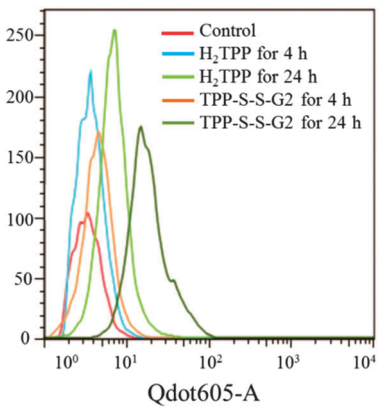

Fig. 9 The cellular uptake of free porphyrin and TPP-S-S-G2 micelles at different times, red line: control, blue line: free porphyrin for 4 h, aqua line: free porphyrin for 24 h, orange line: TPP-S-S-G2 for 4 h, and black green line: TPP-S-S-G2 for 24 h.

porphyrin. With the increase of incubation time to 24 h, the fluorescence intensity increases for free porphyrin and TPP-S-S-G2 micelles, which could be attributed to persistent uptake of these photosensitive agents. It is well known that free porphyrin was transported to cells *via* the passive diffusion mechanism, but the TPP-S-S-G2 micelles may be internalized by an endocytosis process.[58,59]

Confocal laser scanning microscopy was further employed to investigate the cellular uptake of free porphyrin and TPP-S-S-G*n* micelles. MCF-7 cells were cultured with free porphyrin and TPP-S-S-G*n* micelles with a porphyrin concentration of 50 μg mL^{-1} for 4 h and 24 h, respectively. DAPI was used to stain the nucleus after the predetermined interval time. From CLSM results in Fig. 10, the weak fluorescence intensities of free porphyrin and TPP-S-S-G2 micelles were obtained after incubation for 4 h, but the intensities obviously became stronger after incubation for 24 h. Meanwhile, we also found that the fluorescence of TPP-S-S-G2 was also stronger than that of free porphyrin for either 4 h or 24 h. The result indicated that the micelles might be uptaken by a time-dependent process, which is in agreement with the results of flow cytometry mentioned above.

The cellular uptake and intracellular distribution of TPP-S-S-G1 micelles were also evaluated. We obtained a similar result to TPP-S-S-G2, where the fluorescence of TPP-S-S-G1 shifts right

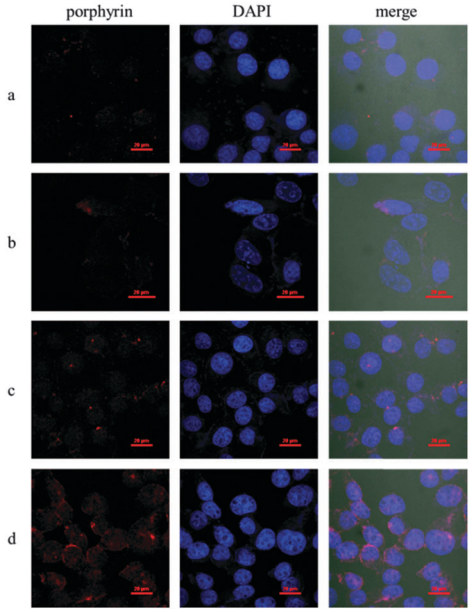

Fig. 10 Confocal laser scanning microscopy images of cellular internalization of free porphyrin and TPP-S-S-G2 micelles with MCF-7 cells (a) free porphyrin for 4 h, (b) free porphyrin for 24 h, (c) TPP-S-S-G2 for 4 h, and (d) TPP-S-S-G2 for 24 h. The images from left to right show porphyrin fluorescence, nuclear staining with DAPI and overlays of images. Scale bar: 20 μm.

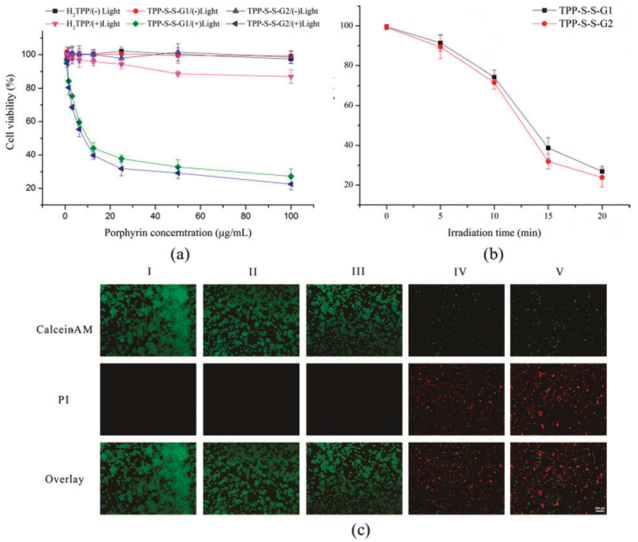

Fig. 11 *In vitro* cytotoxicity of TPP-S-S-G*n* micelles against MCF-7 cells: (a) dark cytotoxicity and phototoxicity at different porphyrin concentrations, (b) the phototoxicity of TPP-S-S-G*n* at different irradiation times, (c) double-staining with calcein AM and PI to detect the PDT efficacy, dead cells: red fluorescence of PI and live cells: green fluorescence of calcein AM, I: control, II: TPP-S-S-G1/light (−), III: TPP-S-S-G2/light(−), IV: TPP-S-S-G1/light(+), V: TPP-S-S-G2/light(+), the porphyrin concentration was 100 μg mL^{-1}, scale bar: 200 μm, and n = 3.

compared to that of free porphyrin at the same incubation time (Fig. S9, ESI†), and the fluorescence intensity was also stronger than that of free porphyrin (Fig. S10, ESI†). However, when comparing the flow cytometry between the two generations, the geometrical mean fluorescence of TPP-S-S-G2 was higher than that of TPP-S-S-G1. This may be because the second generation TPP-S-S-G2 carries more OEG moieties outside as the corona, which could help in cell endocytosis.

Dark cytotoxicity and phototoxicity of TPP-S-S-G*n* micelles

To estimate the PDT efficiency of TPP-S-S-G*n* micelles, we performed *in vitro* phototoxicity with or without light treatment on MCF-7 cells. MTT was used to determine cell viability, and the cells in the dark without treatment were set to a viability of 100% as reference. We first studied the dark cytotoxicity of free porphyrin and TPP-S-S-G*n* micelles. As shown in Fig. 11a, no obvious dark cytotoxicity against MCF-7 cells was observed even at a porphyrin concentration of 100 μg mL^{-1}. Then the phototoxicity was studied by irradiation with visible light LED lamps (400 mW cm^{-2}) for 20 min. For free porphyrin, there was no significant difference between its dark cytotoxicity and phototoxicity, which may be because free porphyrin had low internalization efficiency. However, we found that the phototoxicity of TPP-S-S-G*n* micelles was much higher than that of free porphyrin with the IC50 (calculated for porphyrin concentration) of 9.95 μg mL^{-1} (TPP-S-S-G1) and 8.24 μg mL^{-1} (TPP-S-S-G2), respectively. Actually, the cell viability of these two TPP-S-S-G*n* at a porphyrin concentration of 100 μg mL^{-1} was 27.2% and 22.5%, respectively. Additionally, these two TPP-S-S-G*n* dendrimers exhibited nearly the same phototoxicity, but they were much higher than free porphyrin. We also evaluated the phototoxicity of TPP-S-S-G*n* micelles at different irradiation times ranging from 5, 10, 15 to 20 min at a porphyrin concentration of 100 μg mL^{-1}. As shown in Fig. 11b, the cell viability of cancer cells clearly decreased with increasing irradiation time for TPP-S-S-G1 or TPP-S-S-G2 micelles. The calcein-AM and PI were further employed to stain the cells for direct observation of the PDT efficiency (Fig. 11c). Live and dead cells present were observed as green and red fluorescence using these two dyes, respectively. After MCF-7 cells were treated with TPP-S-S-G*n* micelles for 24 h, there was no red fluorescence detected, indicating that TPP-S-S-G*n* micelles showed no cytotoxicity towards these cells. However, the above MCF-7 cells treated with TPP-S-S-G*n* micelles were irradiated with light for 20 min, and then remarkable red fluorescence appeared as shown in Fig. 11c, which means that the cells were killed by TPP-S-S-G*n* micelles under light irradiation. Thus, the result shows that TPP-S-S-G*n* dendrimers will have potential applications for PDT.

Conclusion

First and second generation of monodisperse amphiphilic dendritic porphyrins TPP-S-S-G1 and TPP-S-S-G2 were efficiently synthesized *via* esterification of porphyrin disulfide and Et-G*n*-OH. Both dendritic porphyrins could self-assemble into spherical micelles in water, and exhibit excellent thermoresponsive behavior with LCSTs between 32.4 °C and 35.8 °C. The disulfide bond in TPP-S-S-G*n* affords them reduction-sensitivity, and their *in vitro* release of reduction-sensitive PSs could be well controlled by DTT. Flow cytometry and CLSM results showed that the cellular uptake of TPP-S-S-G*n* micelles was more than

that of free porphyrin and the uptake process was time-dependent. From MTT assay, TPP-S-S-G*n* micelles were found to exhibit efficient phototoxicity to MCF-7 cells while the free porphyrin showed nearly no toxicity under light irradiation. Therefore, these porphyrin-containing reduction-sensitive dendritic photosensitizers are promising for photodynamic therapy.

Acknowledgements

This work was financially supported by the National Natural Science Foundation of China (No. 51173044), Research Innovation Program of SMEC (No. 14ZZ065), and Shanghai Pujiang Program under 14PJ1402600. W. Z. also acknowledges the support from the Fundamental Research Funds for the Central Universities.

Notes and references

1 T. J. Dougherty, C. J. Gomer, B. W. Henderson, G. Jori, D. Kessel, M. Korbelik, J. Moan and Q. Peng, *J. Natl. Cancer Inst.*, 1998, **90**, 889.
2 M. Ethirajan, Y. Chen, P. Joshi and R. K. Pandey, *Chem. Soc. Rev.*, 2011, **40**, 340.
3 P. Agostinis, K. Berg, K. A. Cengel, T. H. Foster, A. W. Girotti, S. O. Gollnick, S. M. Hahn, M. R. Hamblin, A. Juzeniene, D. Kessel, M. Korbelik, J. Moan, P. Mroz, D. Nowis, J. Piette, B. C. Wilson and J. Golab, *Ca-Cancer J. Clin.*, 2011, **61**, 250.
4 C. Y. Hsu, M. P. Nieh and P. S. Lai, *Chem. Commun.*, 2012, **48**, 9343.
5 C.-S. Lee and K. Na, *Biomacromolecules*, 2014, 4228–4238.
6 H. Nakamura, L. Liao, Y. Hitaka, K. Tsukigawa, V. Subr, J. Fang, K. Ulbrich and H. Maeda, *J. Controlled Release*, 2013, **165**, 191.
7 C. Wang, X. Q. Sun, L. Cheng, S. N. Yin, G. B. Yang, Y. G. Li and Z. Liu, *Adv. Mater.*, 2014, **26**, 4794.
8 J. F. Lovell, T. W. B. Liu, J. Chen and G. Zheng, *Chem. Rev.*, 2010, **110**, 2839.
9 D. E. J. G. J. Dolmans, D. Fukumura and R. K. Jain, *Nat. Rev. Cancer*, 2003, **3**, 380.
10 M. Triesscheijn, P. Baas, J. H. M. Schellens and F. A. Stewart, *Oncologist*, 2006, **11**, 1034.
11 S. H. Voon, L. V. Kiew, H. B. Lee, S. H. Lim, M. I. Noordin, A. Kamkaew, K. Burgess and L. Y. Chung, *Small*, 2014, 4993–5013.
12 C. Ornelas, D. Mery, E. Cloutet, J. R. Aranzaes and D. Astruc, *J. Am. Chem. Soc.*, 2008, **130**, 1495.
13 M. A. Mintzer and M. W. Grinstaff, *Chem. Soc. Rev.*, 2011, **40**, 173.
14 M. Elsabahy and K. L. Wooley, *Chem. Soc. Rev.*, 2012, **41**, 2545.
15 L. Li, K. M. Huh, Y.-K. Lee and S. Y. Kim, *J. Mater. Chem.*, 2011, **21**, 15288.
16 J. Nicolas, S. Mura, D. Brambilla, N. Mackiewicz and P. Couvreur, *Chem. Soc. Rev.*, 2013, **42**, 1147.
17 A. Singh, M. Talekar, T.-H. Tran, A. Samanta, R. Sundaram and M. Amiji, *J. Mater. Chem. B*, 2014, **2**, 8069.
18 D. Luque, A. de la Escosura, J. Snijder, M. Brasch, R. J. Burnley, M. S. T. Koay, J. L. Carrascosa, G. J. L. Wuite, W. H. Roos, A. J. R. Heck, J. J. L. M. Cornelissen, T. Torres and J. R. Caston, *Chem. Sci.*, 2014, **5**, 575.
19 M. Brasch, A. de la Escosura, Y. Ma, C. Uetrecht, A. J. R. Heck, T. Torres and J. J. L. M. Cornelissen, *J. Am. Chem. Soc.*, 2011, **133**, 6878.
20 Y. Cheng, L. Zhao, Y. Li and T. Xu, *Chem. Soc. Rev.*, 2011, **40**, 2673.
21 W.-d. Tian and Y.-q. Ma, *Chem. Soc. Rev.*, 2013, **42**, 705.
22 J. Zhu and X. Shi, *J. Mater. Chem. B*, 2013, **1**, 4199.
23 J. B. Wolinsky and M. W. Grinstaff, *Adv. Drug Delivery Rev.*, 2008, **60**, 1037.
24 D.-L. Jiang and T. Aida, *Chem. Commun.*, 1996, 1523.
25 W. D. Jang, N. Nishiyama, G. D. Zhang, A. Harada, D. L. Jiang, S. Kawauchi, Y. Morimoto, M. Kikuchi, H. Koyama, T. Aida and K. Kataoka, *Angew. Chem., Int. Ed.*, 2005, **44**, 419.
26 W. Li, A. Zhang and A. D. Schluter, *Macromolecules*, 2008, **41**, 43.
27 W. Li, A. Zhang and A. D. Schluter, *Chem. Commun.*, 2008, 5523.
28 Y. F. Guo, Y. N. Zhao, J. Zhao, M. H. Han, A. F. Zhang and X. T. Wang, *Bioconjugate Chem.*, 2014, **25**, 24.
29 H. L. Sun, B. N. Guo, R. Cheng, F. H. Meng, H. Y. Liu and Z. Y. Zhong, *Biomaterials*, 2009, **30**, 6358.
30 B. Khorsand, G. Lapointe, C. Brett and J. K. Oh, *Biomacromolecules*, 2013, **14**, 2103.
31 W. Chen, F. Meng, F. Li, S.-J. Ji and Z. Zhong, *Biomacromolecules*, 2009, **10**, 1727.
32 F. Meng, Z. Zhong and J. Feijen, *Biomacromolecules*, 2009, **10**, 197.
33 N. Rapoport, *Prog. Polym. Sci.*, 2007, **32**, 962.
34 J. Rodríguez-Hernández, F. Chécot, Y. Gnanou and S. Lecommandoux, *Prog. Polym. Sci.*, 2005, **30**, 691.
35 D. Schmaljohann, *Adv. Drug Delivery Rev.*, 2006, **58**, 1655.
36 Y.-Z. You, C.-Y. Hong and C.-Y. Pan, *Macromolecules*, 2009, **42**, 573.
37 R. Savić, L. Luo, A. Eisenberg and D. Maysinger, *Science*, 2003, **300**, 615.
38 J. Ding, J. Chen, D. Li, C. Xiao, J. Zhang, C. He, X. Zhuang and X. Chen, *J. Mater. Chem. B*, 2013, **1**, 69.
39 Z.-Y. Li, J.-J. Hu, Q. Xu, S. Chen, H.-Z. Jia, Y.-X. Sun, R.-X. Zhuo and X.-Z. Zhang, *J. Mater. Chem. B*, 2015, **3**, 39.
40 D. Yue, G. Cheng, Y. He, Y. Nie, Q. Jiang, X. Cai and Z. Gu, *J. Mater. Chem. B*, 2014, **2**, 7210.
41 G. Saito, J. A. Swanson and K.-D. Lee, *Adv. Drug Delivery Rev.*, 2003, **55**, 199.
42 C. Hwang, A. Sinskey and H. Lodish, *Science*, 1992, **257**, 1496.
43 W.-F. Dong, A. Kishimura, Y. Anraku, S. Chuanoi and K. Kataoka, *J. Am. Chem. Soc.*, 2009, **131**, 3804.
44 J. O. Kim, G. Sahay, A. V. Kabanov and T. K. Bronich, *Biomacromolecules*, 2010, **11**, 919.
45 S. H. Kim, J. H. Jeong, S. H. Lee, S. W. Kim and T. G. Park, *J. Controlled Release*, 2006, **116**, 123.

46 E. S. Read and S. P. Armes, *Chem. Commun.*, 2007, 3021.
47 R. Cheng, F. H. Meng, S. B. Ma, H. F. Xu, H. Y. Liu, X. B. Jing and Z. Y. Zhong, *J. Mater. Chem.*, 2011, **21**, 19013.
48 F. H. Meng, W. E. Hennink and Z. Zhong, *Biomaterials*, 2009, **30**, 2180.
49 S. Bolisetty, C. Schneider, F. Polzer, M. Ballauff, W. Li, A. Zhang and A. D. Schlüter, *Macromolecules*, 2009, **42**, 7122.
50 M. H. Nawaz, L. Xu, F. Liu and W. A. Zhang, *RSC Adv.*, 2013, **3**, 9206.
51 Z. Y. Li, H. Y. Wang, C. Li, X. L. Zhang, X. J. Wu, S. Y. Qin, X. Z. Zhang and R. X. Zhuo, *J. Polym. Sci., Part A: Polym. Chem.*, 2011, **49**, 286.
52 G. K. Turner, *Science*, 1964, **146**, 183.
53 J. H. Brannon and D. Magde, *J. Am. Chem. Soc.*, 1980, **102**, 62.
54 A. C. H. Ng, X. Y. Li and D. K. P. Ng, *Macromolecules*, 1999, **32**, 5292.
55 W. Spiller, H. Kliesch, D. Wöhrle, S. Hackbarth, B. Röder and G. Schnurpfeil, *J. Porphyrins Phthalocyanines*, 1998, **02**, 145.
56 Y. Zou, D. E. Brooks and J. N. Kizhakkedathu, *Macromolecules*, 2008, **41**, 5393.
57 G. Karlstroem, A. Carlsson and B. Lindman, *J. Phys. Chem.*, 1990, **94**, 5005.
58 G. Sahay, E. V. Batrakova and A. V. Kabanov, *Bioconjugate Chem.*, 2008, **19**, 2023.
59 H. S. Yoo, K. H. Lee, J. E. Oh and T. G. Park, *J. Controlled Release*, 2000, **68**, 419.